JOURNAL OF SOLID STATE CHEMISTRY 71, 577–581 (1987)

A Large-Angle X-Ray Scattering Study of Two Amorphous Inorganic Polymers, $Ru(SPh)_3$ and $Mo(SPh)_3$

THOMAS VOGT AND JOACHIM STRÄHLE

Institut für Anorganische Chemie, Auf der Morgenstelle 18, D-7400 Tübingen, West Germany

AND ALAIN MOSSET AND JEAN GALY

Laboratoire de Chimie de Coordination du CNRS, Unite n°8241 liée par convention à l'Université Paul Sabatier, 205 route de Narbonne, 31077 Toulouse Cédex, France

Received March 23, 1987

The two inorganic polymers $Ru(SPh)_3$ and $Mo(SPh)_3$ were examined by large-angle X-ray scattering, showing in both cases chains of face-sharing octahedra with alternating metal–metal distances (Ru–Ru: 3.25 and 2.65 Å; Mo–Mo: 3.30 and 2.70 Å). © 1987 Academic Press, Inc.

Introduction

Research in the field of inorganic polymers to obtain materials with new and unusual properties has often been inhibited by the microcrystalline or amorphous nature of these compounds. Hence, structural information is very limited compared with the large number of compounds.

Large-angle X-ray scattering (LAXS) provides a tool which permits investigation of the local order of such compounds and establishment of structural models that may give further insight into organic polymers and their physical properties. The series of amorphous polymers $MM'(EDTA)(H_2O)_4$, $2H_2O$ with M,M' = Ni, Co, Mn, Cu is an example of the correlation between local order and magnetic behavior (*1*).

We present a structural model for the amorphous polymers $Mo(SPh)_3$ and $Ru(SPh)_3$ obtained from LAXS experiments and relate this model to some observed physical properties.

Experimental

Preparation of the Compounds

The synthesis and properties of $Mo(SPh)_3$ and $Ru(SPh)_3$ have been published elsewhere (*2*, *3*). The amorphous powders were carefully crushed, pressed to pellets at 210 kg/cm^2, and mounted on a goniometric head. The structure of each compound has been investigated using the LASIP system built in this laboratory and described elsewhere (*4*, *5*).

0022-4596/87 $3.00

Structural Investigations

Data were collected using the special $\omega - \theta$ diffractometer equipped with a position-sensitive detector for the Mo$K\alpha$ wavelength. The measurements were carried out at room temperature in the transmission mode. Some 2200 equidistant points were measured in 21.5 hr with $1.5° \leq \theta \leq 66°$. Measuring was done in an integrative way to minimize the parallax and nonlinearity problems of the straight linear position-sensitive detector. All 2θ points were *successively* run through all the detector channels. At each angular displacement of the detector an equivalent offset of the channels in the memory is emulated to compensate this movement. This leads to the effect that at a given 2θ angle the scattered intensity is always integrated in the same channel. These data were corrected for background, absorption, polarization, and multiple scattering according to (*6*). Then they were normalized by the method described in (*7*). Atomic scattering factors were taken from Ref. (*8*), Compton scattering factors from Ref. (*9*). Treatment of the experimental data led to the radial distribution function (RDF):

$$F(r) = D(r) - 4\pi\rho_0 r^2. \quad (1)$$

The experimental RDF was obtained using the Zernicke and Prins relation (*10*)

$$D(r) = 4\pi\rho_0 r^2 - \frac{2r}{\pi} \int_{s_{min}}^{s_{max}} si(s)_{exp} M(s) \sin(rs)\, ds \quad (2)$$

where ρ_0 = average electron density, $s = 4\pi(\sin\theta/\lambda)$ (2θ: scattering angle), $i(s)$ = reduced intensities; and $M(s)$ = modification function $M(s) = [f_i^2(0)/f_i^2(s)] \exp(0.01s^2)$. $M(s)$ is used to down-weight inaccurately known high-angle data and to reduce ripples resulting from termination of the integral at s_{max}. Theoretical intensities were calculated according to Debye's formula (*11*)

$$i(s)_{th} = \sum_i \sum_j f_i(s) f_j(s) \frac{\sin(r_{ij}s)}{r_{ij}s} \exp(-b_{ij}s^2) \quad (3)$$

where $i \neq j$, $f(s)$ is the atomic scattering factor, corrected for anomalous scattering, r_{ij} is the distance between two atoms, and b_{ij} is a temperature-related factor influencing the i–j interaction, taking into account both the structural disorder at greater distances and the thermal vibration.

The curve $F(r)_{th}$ is obtained as the Fourier transform:

$$F(r)_{th} = \left(\frac{2r}{\pi}\right) \int_{s_{min}}^{s_{max}} si(s)_{th} M(s) \sin(rs)\, ds. \quad (4)$$

Results and Discussion

The best fit between theoretical and experimental RDFs (Figs. 1 and 2) was obtained using a chain geometry and the following bond lengths and angles:

Ru(S*Ph*)$_3$	Ru–Ru = 3.25 Å;	Ru–S = 2.50 Å	S–Ru–S = 98°
	Ru–Ru = 2.65 Å;	Ru–S = 2.40 Å	S–Ru–S = 112°
			Ru–S–C = 120°
Mo(S*Ph*)$_3$	Mo–Mo = 3.30 Å;	Mo–S = 2.55 Å	S–Mo–S = 99°
	Mo–Mo = 2.70 Å;	Mo–S = 2.45 Å	S–Mo–S = 113°
			Mo–S–C = 120°

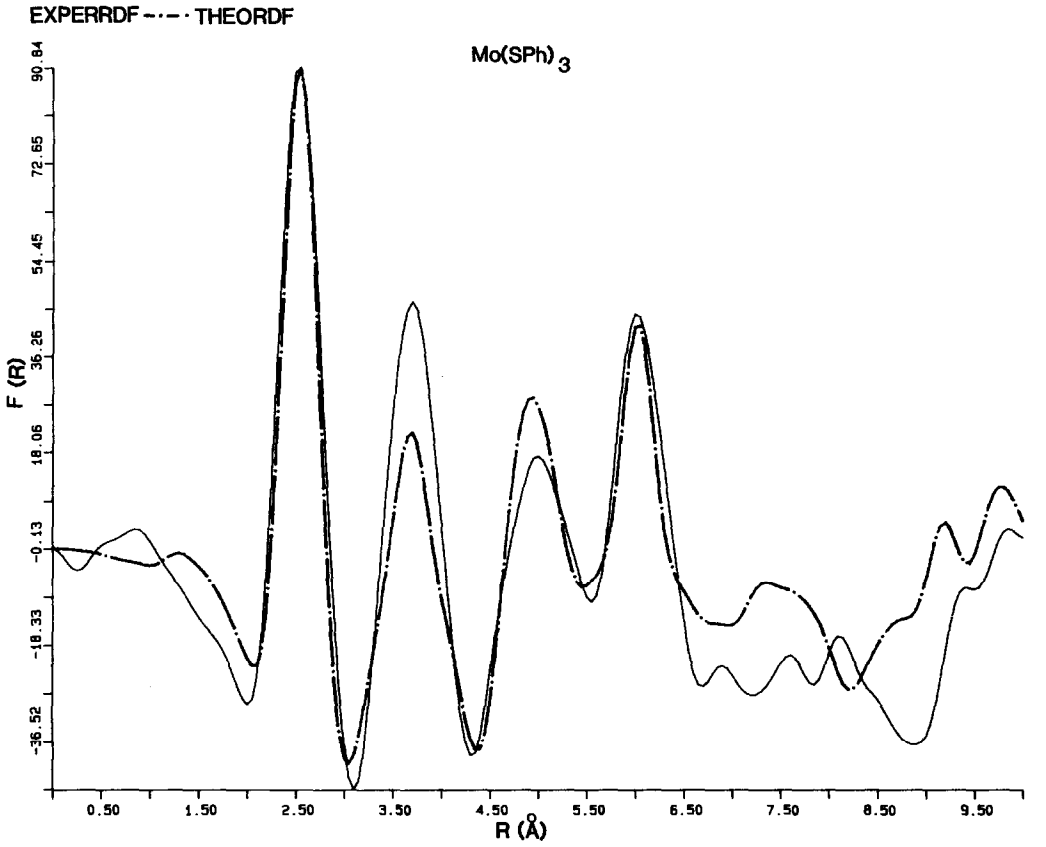

FIG. 1. Experimental (continuous line) and theoretical (broken line) radial distribution curves $F(r)$ of Mo(S*Ph*)$_3$.

The overall geometry is the same as that found in the single-crystal structure analysis of the oligomer $Fe_3(SPh)_6(CO)_6$ described in Ref. (*2*).

The best description of both polymers is obtained on the basis of alternating long and short metal–metal distances leading to a distortion of the octahedral geometry around the metal atoms (Fig. 3). Using an undistorted model with equal *M*–S and *M*–*M* distances, it was not possible to obtain a correct broadness of the first peak, which represents the superposition of the first three coordination spheres around the metal: two sets of each three *M*–S bonds and one *M*–*M* interaction. This observed distortion is in agreement with the vibrational spectrum which shows a splitting of the T_{1u} vibration into two vibrations of types A_{2u} and E_u in the region of the valence vibrations and the appearance of two deformational vibrations as expected for this type of geometry (*2*).

It is interesting to note that Cramer *et al.* (*12*) propose a similar model for amorphous MoS_3 as evidenced by an EXAFS study indicating a short and long Mo–Mo interaction with 2.75 and 3.15 Å and two different Mo–S distances separated by 0.1 Å. The RDF of amorphous MoS_3 investigated by Liang *et al.* (*13*) also shows the first peak at 2.45 Å with a spread of 0.7 Å.

In another study we undertook (*14*) examining the local order of the analogous

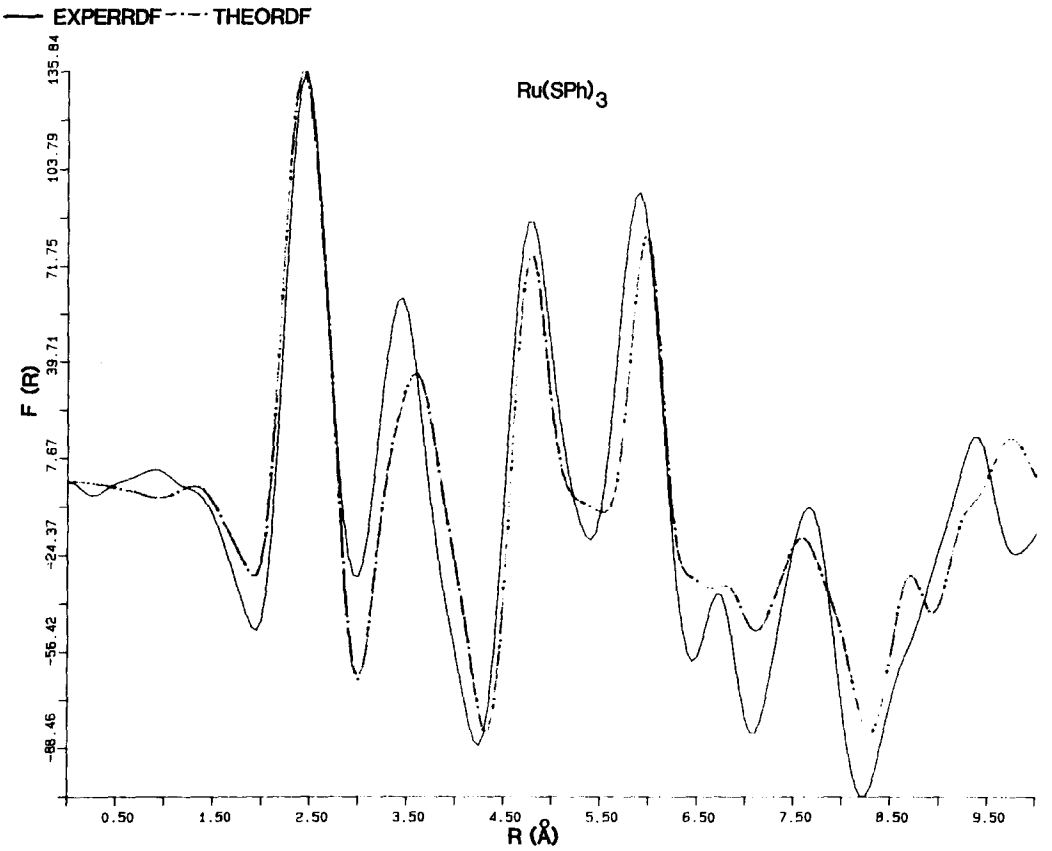

FIG. 2. Experimental (continuous line) and theoretical (broken line) radial distribution curves $F(r)$ of Ru(SPh)$_3$.

Mo(SePh)$_3$ by EXAFS at the Mo K-edge and the Se L-edge and comparing these results with LAXS experiments, we found the same distortion. With this model geometry the weak powder conductivity [1.5×10^{-9} for Mo(SPh)$_3$ and 2×10^{-6} for Ru(SPh)$_3$] can be rationalized that the alternating short and long metal–metal interactions result in a localized bonding behavior rather than in an electron delocalization along the metal–metal chains. Also, the magnetic measurements (*2, 3*) showing magnetic moments of 0.59 BM for Ru(SPh)$_3$ and 1.02 BM for Mo(SPh)$_3$ at 393 K and in both cases a positive susceptibility in the temperature range from 153 to 393 K, which is nearly temperature independent, can reasonably be explained by the pairwise coupling of the metal d electrons in an antiferromagnetic behavior, even though the Néel point is never reached because the

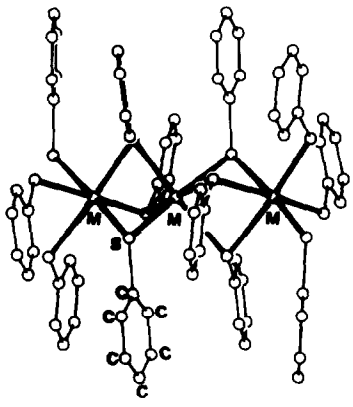

FIG. 3. Partial geometry of the chain $M(SPh)_{3\infty}$.

TABLE I

CORRELATION BETWEEN MAGNETIC MOMENT AND *M–M* DISTANCE

Compound	Magnetic moment (BM)	*M–M* bond distance (Å)	Reference
$MoBr_3$	1.20	2.91	(*15*, *16*)
$Mo(SPh)_3$	1.02	2.70	(*3*), this work
$RuBr_3$	0.50	2.73	(*17*, *18*)
$Ru(SPh)_3$	0.58	2.65	(*3*), this work

compounds decompose beforehand. The correlation between the magnetic moments and the observed metal–metal distances is in good agreement with that observed for the crystalline compounds $RuBr_3$ and $MoBr_3$, as shown in Table I.

References

1. A. MOSSET, J. GALY, E. CORONADO, M. DRILLON, AND D. BELTRAN, *J. Amer. Chem. Soc.* **106,** 2864 (1984).
2. U. BERGER AND J. STRÄHLE, *Z. Anorg. Allg. Chem.* **516,** 19 (1984).
3. U. BERGER, Dissertation, Tübingen (1984).
4. J. GALY, A. MOSSET, AND P. LECANTE, French Patent No. 80.16170, ANVAR (1980); U.K. Patent No. 2081440B (1984); U.S. Patent No. 4.475.225 (1984).
5. P. LECANTE, A. MOSSET, AND J. GALY, *J. Appl. Crystallogr.* **18,** 214 (1985).
6. G. MALET, C. CABOS, A. ESCANDE, AND P. DELORD, *J. Appl. Crystallogr.* **6,** 139 (1973).
7. A. BURIAN, B. RZEPA, P. LECANTE, AND A. MOSSET, *J. Mater. Sci.*, in press.
8. D. T. CROMER AND J. T. WABER, "International Tables for X-ray Crystallography," Vol. IV, Table 2.2.A, Kynoch Press, Birmingham (1974).
9. D. T. CROMER, *J. Chem. Phys.* **50,** 4857 (1969).
10. F. ZERNICKE AND J. A. PRINS, *Z. Phys.* **41,** 184 (1927).
11. P. DEBYE, *Ann. Phys.* **46,** 809 (1915).
12. S. P. CRAMER, K. S. LIANG, A. J. JACOBSON, C. H. CHANG, AND R. R. CHIANELLI, *Inorg. Chem.* **23,** 1215 (1984).
13. K. S. LIANG, J. P. DE NEUFVILLE, A. J. JACOBSON, AND R. R. CHIANELLI, *J. Non-Cryst. Solids* **35,** 1249 (1980).
14. T. VOGT, P. LECANTE, A. MOSSET, J. GALY, AND J. STRÄHLE, paper presented at the IVth International Conference on EXAFS and Near Edge Structure. *J. Phys.* (1987).
15. W. KLEMM AND H. STEINBERG, *Z. Anorg. Allg. Chem.* **227,** 193 (1936).
16. D. BABEL, *J. Solid State Chem.* **4,** 410 (1972).
17. H. K. BREITBACH, Dissertation, Erlangen (1967).
18. K. BRODERSEN, K. H. BREITBACH, AND G. THIELE, *Z. Anorg. Allg. Chem.* **357,** 162 (1968).